

Chapter 7

Theoretical Ab Initio Calculations in Ordered-Vacancy Compounds at High Pressures

A. Muñoz and M. Fuentes-Cabrera

Abstract Ab initio calculations within the Density Functional Theory and the Density Functional Perturbation Theory of the defect chalcopyrite, defect stannite and pseudo-cubic chalcopyrite structures of AB_2X_4 ($X = S$ and Se) compounds are reported. The electronic, dynamical, and elastic properties under hydrostatic pressures are reviewed and discussed in relation with pressure-induced order-disorder phase transitions. Finally, as a matter of example, we present new results of a *first-principles* study of the pressure dependence of several properties for the pseudo-cubic chalcopyrite structure of $CdIn_2Se_4$. We found that the generalized Born stability criteria are violated above 11 GPa, thus PC- $CdIn_2Se_4$ becomes mechanically unstable. Furthermore, we found a phonon dynamical instability around 18 GPa; thus showing that PC- $CdIn_2Se_4$ becomes unstable at high pressures not only from the static but also from the dynamical point of view.

Keywords Ab initio · High pressure · Defect chalcopyrite · Defect stannite · Defect famatinitite · Pseudocubic chalcopyrite · Electronic · Dynamical · Elastic properties

7.1 Introduction

Ordered-vacancy compounds (OVCs) of the $A^{II}B_2^{III}X_4^{VI}$ family are semiconducting materials with potential applications in nonlinear optical and photovoltaic devices. OVCs crystallize in several tetragonal structures (defect chalcopyrite, defect stannite, and pseudocubic structure) derived from the zinc-blende structure. These structures

A. Muñoz (✉)

Departamento de Física Fundamental II, Instituto de Materiales y Nanotecnología,
Universidad de La Laguna, La Laguna, Tenerife, Spain
e-mail: amunoz@ull.edu.es

M. Fuentes-Cabrera

Center for Nanophase Materials Science, Computer Science and Mathematics Division,
Oak Ridge National Laboratory, Oak Ridge, Tennessee 37831, USA
e-mail: fuentescabma@ornl.gov

can be considered as tetrahedrally coordinated if one assumes that they contain an ordered array of stoichiometric vacancies (\square) that compensate the smaller number of cations (A and B) with respect to anions (X). In this way, these compounds can be also formulated as $\square A^{\text{II}}B_2^{\text{III}}X_4^{\text{VI}}$. The effect of the stoichiometric vacancies on the electronic and stability properties of these compounds has been the subject of several theoretical studies.

This chapter will focus on the theoretical studies from *ab initio* methods of the structural, electronic, elastic, and dynamical properties of these compounds under hydrostatic pressure. We will review the high-pressure studies already published for sulphur- and selenium-based OVCs with defect chalcopyrite and defect stannite structures. Furthermore, we will provide, as a matter of example, some new results for CdIn_2Se_4 with pseudocubic structure in order to show how the theoretical methods can be used to study and to predict the dynamical and elastic properties since no high-pressure experimental results are available for this compound to our knowledge.

7.2 Theoretical Background

The state-of-the-art in computational materials science uses the ability of quantum mechanics to predict the total energy of a system of nuclei and electrons. In this respect, *ab initio* calculation techniques only require as input data the atomic number and the chemical composition of the material. With this input it is possible to calculate a variety of properties (electronic, elastic, thermal, vibrational) of any material of interest. In what follows, we give a general introduction to these techniques by focusing on how they have been applied to the study of structural, electronic, dynamical, and elastic properties of $A^{\text{II}}B_2^{\text{III}}X_4^{\text{VI}}$ chalcopyrite compounds under hydrostatic pressure.

The Density Functional Theory (DFT) is an *ab initio* technique that allows the study and prediction of the electronic and structural properties of a material by minimizing its total energy with respect to the nuclear and electronic coordinates. The fundamental variable in this theory is the electronic charge density of the system. The theorem of Hohenberg and Kohn [1] and the seminal work of Khon and Sham [2] are the basis of this theory since they establish that the total energy, $E(V)$, of the ground state of a system is a unique functional of the charge density (and therefore of volume, V), and that this functional is a global (not local) minimum of energy for the correct ground state density. A review on DFT applications can be found in reference [3]. The main approximation in DFT is related to the way in which the contribution to the energy from the effects of the exchange–correlation interactions between electrons is described. The Local Density Approximation (LDA) and the Generalized Gradient Approximation (GGA) are the most popular descriptions currently used [4].

Mujica et al. [5] have reviewed how DFT is applied to the study of the high-pressure phases of many semiconductor compounds. Two different strategies are used to identify the lowest-enthalpy phase of a material as a function of applied pressure.

One strategy consists on minimizing, for a selected set of volumes, the total energy as function of the structural external and internal parameters. It is important to note that pressure, $P(V)$, is a function of volume which is obtained within the DFT formalism at the same time, but independently, as total energy, $E(V)$. The values of pressure (as well others derivatives of the energy) are obtained from the stress theorem [6] which allows also to compute the enthalpy, $H = E + PV$. In the other strategy, the enthalpy is directly minimized at constant pressure. Both strategies provide values for energy, volume, and pressure from where the equation of state (EOS) for a selected structure can be obtained. These techniques, however, have important limitations, the most important one being the existence of many local minima in the configuration space. Many strategies are adopted to overcome this limitation in order to study the high-pressure phases of many materials. For instance, some techniques search the structure of a material at a selected pressure avoiding the imposition of special symmetries, other techniques employ a random search [7], and others employ evolutionary and genetic algorithms [8].

The lattice dynamics of a material and its behavior under high pressure can be analyzed by DFT or by the Density Functional Perturbation Theory (DFPT) [9]. DFPT requires the calculation of the ground state charge density and its linear response to external excitations. This permits, among other interesting quantities, to obtain the elastic properties and the phonon dispersion along the whole Brillouin zone. In particular, this technique is interesting for the study of phonons in polar materials, which are more complex from the theoretical point of view, since the long range of the Coulomb interactions gives rise to a macroscopic electric field, and phonons in polar materials are coupled to this macroscopic electric field. This effect is reflected in the appearance in polar materials of different values for the frequencies of the transversal optic (TO) and the longitudinal optic (LO) phonons at the zone center (Γ point) of the Brillouin zone; i.e., the so-called LO–TO splitting. This splitting can be calculated by means of the Born effective charge tensor Z^* and the electronic dielectric constant ϵ_∞ . To take these two variables into account for the calculation of the LO–TO splitting, DFPT requires the study of the electron density response to an homogeneous electric field allowing to obtain the LO–TO splitting near the Γ point (along the [100] or [010] and [001] directions in OVCs).

Phonon frequencies can be also calculated from energy differences using DFT instead of DFPT. In DFT, phonon frequencies are obtained producing small finite displacements of a few atoms in a periodic crystal at equilibrium. In this methodology, one begins with the equilibrium structure at a certain pressure and produces a distortion by displacing a single atom by a small amount U_0 (typically 0.2 Å in OVCs). The atomic forces that result from this distortion are then computed, and the ratio of these forces and U_0 gives one complete row of the force-constants matrix. Subsequently, symmetry operations are applied to these rows to produce the complete matrix. Within the harmonic approximation, this method is exact, yet anharmonic effects are avoided by averaging the results with displacements $+U_0$ and $-U_0$. This approach, named the frozen-phonon approach or direct method, permits to calculate a phonon vibration at a selected wave vector, q [10, 11]. In this method, the study of phonons in polar materials is not straightforward, as in DFPT, because the non-

analytic term related with the electric field is not included in the dynamical matrix at the Γ point, so only frequencies of TO modes are obtained; i.e., the LO-TO splitting is not provided. However, the LO-TO splitting can be obtained a posteriori if the Born effective charge tensor and the macroscopic dielectric constant are calculated from ab initio. In summary, the direct method approach can be used for the calculation of the phonon dispersion but is limited by the size of the system under study when the size of the supercell increases. Its advantage relies on how easy it is to implement.

Since Raman and infrared spectra provide information of phonon frequencies at the Γ point, these frequencies can be computed either with DFPT or with the direct method approach. The study of the vibrational spectra of the material under pressure can provide many interesting properties of the compound under study. For example, the presence of soft modes could be related with phase transitions [9]. Furthermore, using simple models to describe the electron-phonon interactions it is possible to calculate the temperature dependence of the electronic band gap [12].

Elastic constants are interesting to know the elastic or mechanical properties of materials. The elastic properties provide, not only information concerning the strength of the material, they also provide important insight into the interatomic potentials, EOS, and other elastic quantities (Young modulus, shear modulus, etc.) which are interesting for material engineering. The pressure behavior of the elastic constants of a material in a certain structure gives information concerning the mechanical stability of that material under pressure and its possible relation with the structural transformations. These constants can be viewed as force constants associated to a homogeneous strain applied to the material. In fact, the calculation of the elastic constants is performed by studying the response of the periodic system to a microscopic distortion. In order to obtain the elastic constants from ab initio methods, again DFPT is used to calculate the elastic constants tensor.

7.3 Structural Considerations

As already commented, $A^{\text{II}}B_2^{\text{III}}X_4^{\text{VI}}$ compounds (with A and B divalent and trivalent metals, respectively and $X = \text{S, Se}$) known as ordered vacancy compounds crystallize in different tetragonal structures deriving from the zinc-blende structure. In fact, they are variants of the tetrahedrally-bonded tetragonal chalcopyrite structure which is common to materials of chemical composition $A^{\text{II}}B^{\text{IV}}X_2^{\text{V}}$ and $A^{\text{I}}B^{\text{III}}X_2^{\text{VI}}$. Different crystal structures with slightly different ordering of the cations and vacancies as well as order-disorder transition phases exist in this type of compounds. Excellent works related with these materials can be found in the review of Georgobiani et al. [13] and in the paper of Bernard and Zunger [14].

OVCs of the $A^{\text{II}}B_2^{\text{III}}X_4^{\text{VI}}$ family crystallize in three different tetragonal phases: the defect chalcopyrite (DC) structure (space group I-4, No. 82), also known as thiogallate structure, the defect stannite (DS) structure, also known as defect famatinite, (space group I-42m, No. 121), and the ordered pseudo-cubic structure (PC) (space group P-42m, No. 111). The DC and DS structures are defective-like

chalcopyrite structures with different degrees of cation disorder which have seven atoms and one vacancy per unit cell. If the vacancy is considered as an atom, then each atom is surrounded by four neighbors in a tetrahedral-like environment. For details and pictures of all these structures we refer the readers to the two previous chapters of this book.

7.4 Electronic Band Structure and Optical Properties

As already commented, $A^{II}B_2^{III}X_4^{VI}$ materials are interesting for nonlinear frequency conversion applications and nonlinear optical devices and some of them have been proposed for phase change memories to replace actual flash memories. The reduction of the cubic T_d symmetry in zinc-blende-type crystals to the tetragonal symmetry D_{2d} in chalcopyrite-type and defect chalcopyrite-type crystals is the origin of birefringent behavior and the reason for the nonlinear properties of these semiconductors [14]. Thus, their electronic band structures and their evolution under pressure have been the subject of numerous experimental and theoretical studies. It is well known that DFT systematically underestimates the band gap and that different exchange-correlation functional provides different values of the band gap, yet the pressure evolution and the symmetry of the band gap are usually well described [15]. As the theoretical techniques improved, many OVCs of the $A^{II}B_2^{III}X_4^{VI}$ family have been studied and their electronic properties have been compared to experiments when possible. In what follows, we briefly describe some of the most interesting studies on the electronic properties of these compounds.

One of the earliest theoretical studies on the electronic properties is that of Baldereschi et al. [16]. In 1977, they used a pseudopotential method to investigate the electronic properties of PC- $CdIn_2Se_4$. The character and value of the calculated band gap were in agreement with previous experiments, yet an intra-valence gap was found. In 1988, Bernard and Zunger [14] used an all-electron potential-variation mixed-basis approach to investigate the structure and electronic properties of the same material. This study revealed that the vacancy has associated with it lone-pair Se dangling orbitals which are oriented in different directions and form a disperse band occupying the uppermost part of the valence band. However, unlike Baldereschi et al. [16], an intra-valence gap was not found. Subsequently, Marinelli et al. [17] using DFT-LDA and norm-conserving pseudopotentials studied the PC and spinel (space group $Fd-3m$, No. 227) structures of $CdIn_2Se_4$ at equilibrium pressure. For the PC structure, they did not find an intra-valence gap, either.

Of the theoretical studies, the most comprehensive ones are those of Jiang and Lambrecht [18] and Mishra and Ganguli [19]. They studied the materials $A^{II}B_2^{III}X_4^{VI}$ ($A = Zn, Cd, Hg$; $B = Al, Ga, In$; $X = S, Se, Te$) and AAI_2Se_4 ($A = Ag, Cu, Cd, Zn$), respectively. Noteworthy, Jiang and Lambrecht [18] used an empirical correction for the band gaps that improved the agreement with experimental data. This work reports the band structure and the band gap of many compounds with DC

structure and the authors examined the chemical trends for the bands gaps and the relations with the possible nonlinear optical applications.

DC-CdAl₂Se₄ was studied by Fuentes Cabrera and Sankey [20], using total energy pseudopotential calculations with the LDA functional parametrized by Perdew and Zunger [21], and the GGA functional in the Perdew and Wang approximation [22] for the exchange correlation potential. They studied the DC and the spinel phases and showed that the DC phase has a direct gap while the spinel phase has an indirect gap. Using a Generalized Density Functional Theory (GDFT) correction [23], the calculated band gap of the DC phase was found in excellent agreement with experiments. These authors also showed that DC and spinel structures have practically the same energy when the LDA functional is used, whereas the DC phase is more stable than the spinel structure, as is experimentally found, when the GGA functional is used. Recently, Ourani et al. have studied the same compound by means of the full potential linearized augmented plane waves (FP-LAPW) [24]. Using the Engel-Vosko GGA functional (EV-GGA) [25], they found a direct band gap very close to the 3.07 eV experimental band gap. Verma et al. [26] analyzed the pressure and temperature evolution of direct and indirect band gaps of this compound, using FP-LAPW method, and considering the effect of employing different exchange-correlation functionals (LDA [20], Perdew–Burke–Ernzenhoff (GGA-PBE) [27], and GGA and the EV-GGA [25]). Calculations with EV-GGA were found to reproduce well the value of the experimental band gap.

The electronic and optical properties of ZnAl₂Se₄ have been reported by Verma et al. [28] calculated with the FP-LAPW method and two different functionals for the exchange-correlation potential (GGA-PBE [27] and EV-GGA [25]). They concluded that ZnAl₂Se₄ is a direct wide band gap material and that both the direct and indirect band gaps increase with pressure. The optical properties were also reported showing a considerable anisotropy.

The trends of the band gap pressure coefficients of the family compounds ZnGa₂X₄ (X = S, Se, Te) have been studied by Jiang et al. [29] using the LDA functional to describe the exchange-correlation potential with the pseudopotential plane wave method. They found that DC and DS phases have different band gaps. Ouahrani et al. [30] have made a study of the AAl₂Se₄ compounds (A = Zn, Cd, and Hg) within the DFT and the GW quasi-particle approximation to correct the DFT band gap underestimation, with emphasis in the influence between nonlinear optical properties and the ionicity degree.

Singh et al. investigated the electronic and optical properties of DC-HgAl₂Se₄ using the FP-LAPW method with LDA, GGA, GGA-PBE, and EV-GGA exchange-correlation functionals [31]. They also included the spin-orbit coupling in the calculations and showed that this reproduces the structural parameters better than EV-GGA. However, EV-GGA gives a band gap in excellent agreement with experimental results. The real and imaginary part of the dielectric function was also reported, showing considerable anisotropy of optical properties. Similarly, Reshak et al. investigated DC-HgGa₂S₄ with the FP-LAPW method and different exchange correlation functionals (LDA, GGA, and EVGGA) to study the band gap [32]. Once again, it was

found that EV-GGA functional gives a direct band gap of 2.84 eV in good agreement with the experiments.

Lavrentyev et al. performed ab initio calculations and X-ray photoelectron spectroscopy, to study DC-CdGa₂S₄ and DC-CdGa₂Se₄ compounds [33–35]. They reported a direct band gap in CdGa₂Se₄ and the real and imaginary part of the electronic dielectric function that evidence considerable anisotropy. For CdGa₂S₄, employing an ab initio full Multiple scattering code, they obtained the theoretical form of the X-ray absorption spectra and the density of states which reveals how the form of the edge of conduction band is determined mainly by Ga *s*-states.

Fuentes-Cabrera et al. investigated the dependence of the band-gap with pressure of DC-CdGa₂S₄ and DC-CdGa₂Se₄ without the inclusion of disorder in the structure [36]. The band gap showed a parabolic behavior: as the pressure increased, the band gap reached a maximum and then it started to decrease. The strong nonlinear pressure dependence of the optical band gap in DC-CdGa₂Se₄ and DC-HgGa₂Se₄ and other OVCs was studied experimentally and theoretically (with DFT calculations using the GGA-PBE functional) by Manjón et al. [37]. The strong nonlinear behavior of the direct band gap was found to be due to a band anti-crossing at the Γ point caused by the presence of ordered stoichiometric vacancies in OVCs. Therefore, it was proposed that this nonlinear behavior of the direct band gap is a general characteristic of the adamantine-type OVCs of the B₂^{III}X₃^{VI} and A^{II}B₂^{III}X₄^{VI} families. A similar experimental and theoretical study of the pressure dependence of the band gap was performed by Gomis et al. in DC-CdGa₂Se₄ [38]. The dependence of the band gap under pressure showed a parabolic behavior as in [36]. However, the experimental and the theoretical dependence showed a disagreement at high pressures. This was interpreted as an indication that order–disorder transitions (not considered in calculations) were taking place. That is, it was argued that as the order–disorder transitions consisting of cation or cation–vacancy disorder were not accounted for by theory (since in these calculations the structures remained always ordered with cations and vacancies at fixed positions), so they were the reason for the disagreement between theory and experiment.

In both references [14] and [16], it was suggested that the stoichiometric vacancies play a determinant role on the structural properties of these materials. This would explain why for some of these compounds it is, generally, impossible to determine unequivocally whether they are in an ordered stannite (or famatinite) or in a defect chalcopyrite structure at room temperature. In this respect, Bernard and Zunger [14] discussed a number of possible order–disorder transitions, and even identified two stages of disordering. These disordering transitions are discussed in the next section.

7.5 Vibrational Properties Under Hydrostatic Pressure

Some empirical methods can be also employed in the study of the dynamical properties of materials. Lattice dynamical calculations of DC-AGa₂X₄ (A = Cd, Hg; X = S, Se) compounds were performed by Ohrendorf et al. using a short-range

force model; i.e., an empirical model [39]. The work discusses the problems related with the long range interactions, and how the force parameters, used in the study of vibrational properties, are affected. In what follows, we will concentrate only in the theoretical ab initio studies of the vibrational properties.

The primitive unit cell of tetragonal DC and DS structures contains one formula unit, i.e., 7 atoms. As commented in the two previous chapters, there are 21 normal modes of vibration, of which 3 are acoustic and 18 are optical modes. According to group theory, the irreducible representations of phonon modes at the Γ point for the DC structure are:

$$\Gamma : 3A(\text{R}) \oplus 6B(\text{R}, \text{IR}) \oplus 6E(\text{R}, \text{IR})$$

where R means that the mode is Raman active and IR that it is infrared active. The A modes are non-polar, and the B and E (doubly degenerated) are polar modes. This results in 13 Raman-active modes ($3A \oplus 5B \oplus 5E$), 10 IR-active modes ($5B \oplus 5E$), and 3 acoustic modes ($B \oplus E$). On the other hand, the ordered DS structure (model 1 in Table 5.2) has also 21 phonon modes at the Γ zone center point with the following mechanical representation:

$$\Gamma : 2A_1(\text{R}) \oplus A_2(\text{R}, \text{IR}) \oplus 2B_1(\text{R}) \oplus 4B_2(\text{R}, \text{IR}) \oplus 6E(\text{R}, \text{IR})$$

where B_2 and E are polar modes. This gives 12 Raman-active modes ($2A_1 \oplus 2B_1 \oplus 3B_2 \oplus 5E$), 8 IR-active modes ($3B_2 \oplus 5E$), 3 acoustic modes (B_2 and E), and one silent mode A_2 . Since polar modes have a LO–TO splitting, this means that the DC structure has 23 Raman-active modes and the DS structure has 20 Raman-active modes.

In 1988, Bernard and Zunger suggested that the vacancies play a determinant role in the structural properties of $A^{\text{II}}B_2^{\text{III}}X_4^{\text{VI}}$ OVCs [14]. In particular, they discussed a number of possible order–disorder transitions and proposed two stages of disordering upon increasing temperature. In the first stage, the two cations A and B mutually substitute for one another; in the second stage, the two cations and the vacancy disorder mutually. Such transitions would explain why for some of these compounds it is generally unequivocally impossible to determine whether they are in an ordered stannite (or famatinite) or in a defect chalcopyrite structure at room temperature.

In 1999, Ursaki et al. used Raman spectroscopy under hydrostatic pressure to investigate the compounds AGa_2X_4 ($A = \text{Cd}, \text{Zn}; X = \text{S}, \text{Se}$) [40]. The compounds with Cd crystallize in the DC structure, whereas those with Zn crystallize in the DS structure (model 6 in Table 5.2 with partial disorder in the cation sublattice). Ursaki et al. proposed that all these compounds undergo the two stages of pressure-induced disordering already proposed by Bernard and Zunger for temperature-induced disordering. They suggested that in the DC compounds the first stage involved a disordering among the Cd and Ga cations (thus leading to the DS structure as commented in [41]). This stage could also occur for the compounds with the DS structure having model 6 in Table 5.2 and [41], where Zn and Ga atoms are already partially disordered, if one considers that both Zn and Ga atoms can become totally disordered to

give the DS structure (model 2 in Table 5.2 and [41]). The first stage of disordering was proposed to be characterized by the tetragonal distortion of the initial structures. In the second stage of disordering, vacancies are involved in the disordering with cations giving rise to a disordered zinc-blende (DZ) structure prior to the phase transition to the Raman-inactive disordered rocksalt (DR) structure. Unfortunately, Raman spectra of the DZ phase have not been found prior to the transition from either DC or DS compounds to the DR phase yet. Therefore, the existence of these two stages of pressure-induced disorder have been recently questioned by the group of Manjón et al. in several papers which support only the existence of the first stage of disorder and the direct transition from the DS structures to the DR phase [38, 42, 43].

In 2001, Fuentes-Cabrera used DFT-LDA calculations to investigate the Raman spectra under hydrostatic pressure of the compounds DC-CdGa₂X₄ (X = S, Se) [36]. The LO–TO splitting was not taken into account in this study. The results were subsequently fitted to the polynomial, i.e. $\omega = \omega_0 + aP + bP^2$, where ω is frequency and P is pressure; this is the same polynomial considered by Ursaki et al. [40]. A good agreement was found in the comparison of the experimental and theoretical Raman frequencies at different pressures. This was also true even for the *A* and *E* modes, whose changes in width were considered as the signals for the first stage of pressure-induced phase transitions. The agreement of the frequencies at different pressures was surprising because in the theoretical calculations the structures were not disordered at all, whereas Ursaki et al. suggested several order–disorder transitions caused by the two-stages of disordering proposed by Bernard and Zunger. This data along with the theoretical dependence of the band gap with pressure [36] offer one more piece of the puzzle, and could be compared with future experimental studies to settle the argument of whether order–disordering transitions were or not taking place under hydrostatic pressure.

In a subsequent study, Gomis et al. measured and calculated, using ab initio techniques, the optical and vibrational spectra of DC-CdGa₂Se₄ under pressure [38]. Raman scattering measurements complemented with the lattice dynamics calculations allowed to assign and to discuss the symmetries of the Raman-active modes up to 22 GPa. In general, a good agreement between experimental and theoretical phonon frequencies was found along the whole pressure range.

Vilaplana et al. performed recently experiments and ab initio DFPT calculations to evaluate the vibrational properties of DC-ZnGa₂Se₄, DS-ZnGa₂Se₄, DC-HgGa₂Se₄, and DC-HgGa₂S₄ under pressure [42–44]. Pure *B* and *E* modes with TO and LO splitting were obtained which could be compared to experimental values. Tables 7.1, 7.2 show the experimental and theoretical Raman mode frequencies of Raman-active optical modes and the pressure coefficients for DC-HgGa₂Se₄ and DC-HgGa₂S₄, respectively. Figures 7.1 and 7.2 show the theoretical and experimental Raman-active modes as function of pressure of DS and DC phases of ZnGa₂Se₄ respectively. It must be noted that the theoretical DS structure was calculated with the 4*d* sites occupied by Ga (model 1 in Table 5.2 and [41]) to be compared with the experimental DS structure where Zn and Ga are mixed in 4*d* sites (model 6 in Table 5.2 and [41]) because of the computationally expensive task of performing calculations of disordered phases

Table 7.1 Experimental and theoretical Raman mode frequencies and their pressure coefficients in DC-HgG₂Se₄ at zero pressure using $\omega(P) = \omega_0 + a_1 P + a_2 P^2$

Mode symmetry	ω_0^a [cm ⁻¹]	a_1^a [cm ⁻¹ GPa ⁻¹]	$a_2^a \times 100$ [cm ⁻¹ GPa ⁻²]	ω_0^b [cm ⁻¹]	a_1^b [cm ⁻¹ GPa ⁻¹]	$a_2^b \times 100$ [cm ⁻¹ GPa ⁻²]
E _{TO} ¹	51.1	0.30	-2.3	49.1	0.26	-2.9
E _{LO} ¹				53.0	-0.02	-2.2
B _{TO} ¹	54.7	1.50	-2.1	49.9	1.73	-2.7
B _{LO} ¹				50.9	1.60	-2.3
E _{TO} ²	100.1	0.03	-0.8	94.9	-0.13	
E _{LO} ²				95.0	-0.13	
B _{TO} ²	119.5	0.07	5.9	116.0	-0.10	
B _{LO} ²				119.3	-0.26	
A ¹	139.2	4.72	-7.3	126.8	4.53	-5.1
E _{TO} ³	157.8	4.66	-8.5	143.8	4.65	-7.2
E _{LO} ³				150.9	4.54	-6.7
B _{TO} ³	176.4	4.72	-10.6	161.2	4.55	-6.6
B _{LO} ³				169.1	4.86	-7.4
A ²	182.6	4.45	-18.0	165.4	4.00	-6.5
A ³	205.4	2.86	-3.6	185.0	2.97	-2.6
B _{TO} ⁴	216.3	2.01	0.4	198.6	2.04	0.5
B _{LO} ⁴				213.9	1.91	-0.2
E _{TO} ⁴	235.8	4.17	-7.6	215.9	4.71	-7.5
E _{LO} ⁴				224.8	4.43	-6.4
E _{TO} ⁵	242.8	4.47	-9.7	232.3	3.61	-3.7
E _{LO} ⁵	271.5	2.54	-2.85	249.9	3.48	-4.7
B _{TO} ⁵	272.3	4.90	-5.94	240.4	6.60	-10.3
B _{LO} ⁵	288.4	3.08	-0.92	252.7	6.07	-9.0

^a Experimental Raman data^b Theoretical calculations

with ab initio techniques. These results are a clear example of how the ab initio calculations can help to identify the different Raman modes and the reasonable agreement between the theoretical data and the experimental results.

7.6 Elastic Properties Under Pressure

The study of the elastic properties of ternary chalcopyrite compounds with ab initio methods was also applied to A^{II}B₂^{III}X₄^{VI} compounds. It must be noted that very few ab initio theoretical studies of elastic properties are available for these materials.

Compounds crystallizing in the DC (I-4) structure belong to the tetragonal Laue group TII. This Laue group contains all crystals with 4, $\bar{4}$ and $4/m$ point groups. In this group there are seven independent elastic constants which are:

Table 7.2 Experimental (exp.) and calculated (th.) Raman-mode frequencies at room pressure and their pressure coefficients in DC-HgGa₂S₄ as obtained from fits to the data using ($\omega = \omega_0 + aP$) or ($\omega = \omega_0 + aP + bP^2$) equations

Mode symmetry (th.)	ω_0 (th.) (cm ⁻¹)	a (th.) (cm ⁻¹ GPa ⁻¹)	b (th.) × 100 (cm ⁻¹ GPa ⁻²)	Mode symmetry (exp.)	ω_0 (exp.) (cm ⁻¹)	a (exp.) (cm ⁻¹ GPa ⁻¹)	b (exp.) × 100 (cm ⁻¹ GPa ⁻²)
E ¹ (TO)	64(1)	-0.14(3)		E ¹ (TO)	62(1)	0.16(3)	
E ¹ (LO)	68(1)	-0.3(1)		E ¹ (LO)	65(1)	0.10(1)	
B ¹ (TO)	61(1)	1.4(1)		B ¹ (TO)	61(1)	1.3(5)	
B ¹ (LO)	62(1)	1.3(1)		B ¹ (LO)			
E ² (TO)	128(1)	-0.14(4)		E ² (TO)	133(1)	0.04(2)	
E ² (LO)	129(1)	-0.16(3)		E ² (LO)			
B ² (TO)	155(1)	-0.3(1)		B ² (TO)	163(1)	-0.2(1)	
B ² (LO)	162(1)	-0.5(1)		B ² (LO)			
A ¹	216(2)	6.6(3)	-8(2)	A ¹	220(1)	7.0(1)	-10(2)
E ³ (TO)	229(2)	6.0(3)	-10(3)	E ³ (TO)	230(2)	6.3(1)	-12(2)
E ³ (LO)	236(2)	5.9(3)	-8(2)	E ³ (LO)			
B ³ (TO)	237(2)	6.1(3)	-9(2)	B ³ (TO)			
B ³ (LO)	253(2)	5.2(3)	-7(2)	B ³ (LO)			
A ²	299(2)	5.0(3)	-7(2)	A ²	300(2)	5.1(1)	-7(1)
B ⁴ (TO)	305(2)	1.8(1)	1.9(1)	B ⁴ (TO)	316(3)	3.0(1)	-2(1)
B ⁴ (LO)	326(2)	3.1(2)	-3(1)	B ⁴ (LO)			
E ⁴ (TO)	307(2)	4.6(2)	-6(2)	E ⁴ (TO)	315(4)	4.9(3)	-7(1)
E ⁴ (LO)	336(2)	3.8(2)	-6(2)	E ⁴ (LO)	341(3)	3.9(2)	-6(1)
A ³	342(2)	3.3(2)	-3(1)	A ³	358(2)	3.7(1)	-6(1)
E ⁵ (TO)	349(2)	3.8(2)	-4(1)	E ⁵ (TO)	360(3)	4.3(2)	-6(1)
E ⁵ (LO)	362(2)	4.0(2)	-5(1)	E ⁵ (LO)	364(3)	3.2(2)	-10(2)
B ⁵ (TO)	364(2)	6.7(3)	-8(2)	B ⁵ (TO)	387(4)	6.1(3)	-9(2)
B ⁵ (LO)	378(2)	6.0(3)	-7(2)	B ⁵ (LO)			

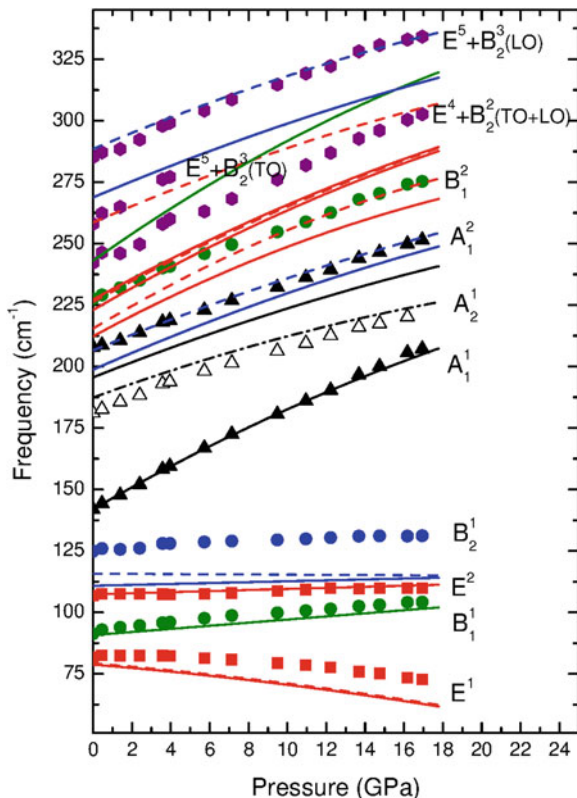


Fig. 7.1 Pressure dependence of the experimental (*symbols*) and calculated (*lines*) vibrational modes in DS-ZnGa₂Se₄

C_{11} , C_{12} , C_{13} , C_{33} , C_{44} , C_{66} , and C_{16} [45]. On the other hand, the DS (I-42m) and PC (P-42m) structures belong to the tetragonal Laue group TI, which contains all crystals with 422 , $4mm$, $-42m$ and $4/mmm$ point groups. In this group there are six independent second-order elastic constants which are: C'_{11} , C'_{12} , C'_{13} , C'_{33} , C'_{44} , and C'_{66} [45]. It is possible to transform the seven components C_{ij} of the elastic tensor of a TII crystal into the six components C'_{ij} of the elastic tensor of a TI crystal. For that purpose it is necessary to make C'_{16} equal to zero by means of a rotation around the z axis [46].

Gomis et al. recently performed a theoretical study of the elastic properties of DC-HgGa₂Se₄ under pressure [47], using the pseudopotential plane wave method with the GGA PBEsol [48] functional to describe the exchange correlation energy. Table 7.3 shows the set of seven elastic constants C_{ij} obtained at zero pressure together with the two sets of six C'_{ij} obtained after applying the corresponding rotations. The table also includes previous theoretical results for the seven C_{ij} elastic constants of DC-CdGa₂Se₄ and DC-CdGa₂S₄ [49].

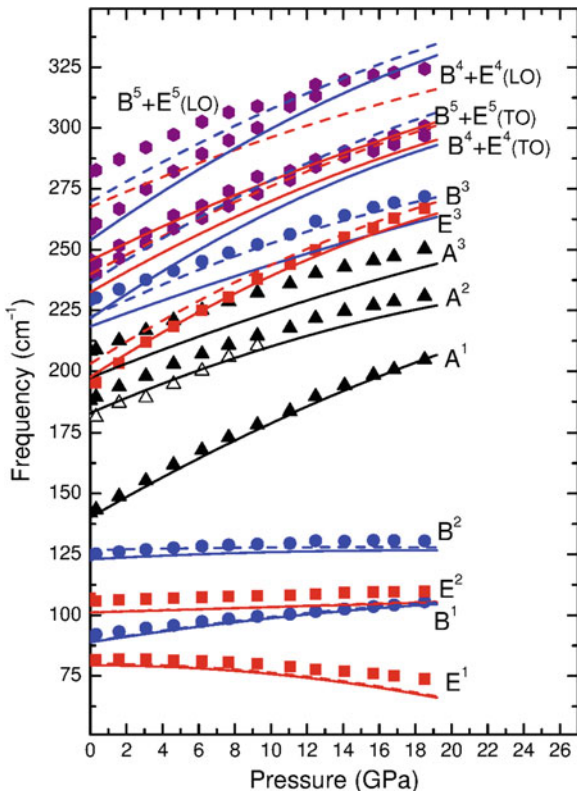


Fig. 7.2 Pressure dependence of the experimental (*symbols*) and calculated (*lines*) vibrational modes in DC-ZnGa₂Se₄

From the elastic constants it is possible to obtain, using standard formulas, the bulk modulus, B , and the shear modulus, G , for the tetragonal Laue group TI. Three different approximations are used in order to calculate the bulk and shear modulus, they are known as the Voigt [50], Reuss [51] and Hill [52] approximations, labeled with subscripts V , R , and H , respectively, defined by the following equations:

$$B_V = \frac{2C_{11} + C_{33} + 2C_{12} + 4C_{13}}{9} \quad (7.1)$$

$$B_R = \frac{1}{2S_{11} + S_{33} + 2S_{12} + 4S_{13}} \quad (7.2)$$

$$B_H = \frac{B_V + B_R}{2} \quad (7.3)$$

Table 7.3 The C_{ij} elastic constants (in GPa) for DC-HgGa₂Se₄

	DC-HgGa ₂ Se ₄	DC-CdGa ₂ Se ₄ ^a	DC-CdGa ₂ S ₄ ^a
C_{11}	54.2	52.5	61.8
C_{12}	24.3	20.4	24.7
C_{13}	31.2	38.8	35.7
C_{33}	55.5	60.0	50.0
C_{44}	29.9	31.6	33.9
C_{66}	26.2	16.0	27.0
C_{16}	-0.3	-1.9	-2.7
C'_{11}	54.2 ^b , 65.5 ^c		
C'_{12}	24.3 ^b , 13.0 ^c		
C'_{13}	31.2 ^b , 31.2 ^c		
C'_{33}	55.5 ^b , 55.5 ^c		
C'_{44}	29.9 ^b , 29.9 ^c		
C'_{66}	26.2 ^b , 14.9 ^c		
B_V, B_R, B_H	37.5, 37.2, 37.4	36.1 ^d	58.4 ^d
G_V, G_R, G_H	22.3, 18.8, 20.6		
Y_V, Y_R, Y_H	55.9, 48.4, 52.2		
ν_V, ν_R, ν_H	0.25, 0.28, 0.27		
$B_V/G_V, B_R/G_R, B_H/G_H$	1.68, 1.98, 1.81		
A	1.75 ^c , 0.57 ^d		

The set of elastic C'_{ij} constants (after rotation for two different angles) are also given. The elastic moduli B, G, and Y (in GPa) and Poisson's ratio (ν) are given in the Voigt, Reuss and Hill approximations. The B/G ratio and the shear anisotropy factor (A) are also given

^a C_{ij} data from [48]

^{b,c} Rotation angle of $\phi_x = 0.76^\circ$ and $\phi_y = 45.76^\circ$, respectively

^d Obtained for B_R a value 40.6 GPa from the C_{ij} data from [48]

$$G_V = \frac{2C_{11} + C_{33} - C_{12} - 2C_{13} + 6C_{44} + 3C_{66}}{15} \quad (7.4)$$

$$G_R = \frac{15}{8S_{11} + 4S_{33} - 4S_{12} - 8S_{13} + 6S_{44} + 3S_{66}} \quad (7.5)$$

$$G_H = \frac{G_V + G_R}{2} \quad (7.6)$$

where S_{ij} are the components of the elastic compliance tensor (the inverse of the elastic constants tensor).

Other interesting elastic quantities are the Young modulus (Y) and the Poisson's ratio (ν) defined by:

$$Y_Z = \frac{9B_Z G_Z}{G_Z + 3B_Z} \quad (7.7)$$

$$\nu_Z = \frac{1}{2} \left(\frac{3B_Z - 2G_Z}{3B_Z + G_Z} \right) \quad (7.8)$$

where the subscript Z refers to the symbols V , R , and H , respectively. Table 7.3 reports the values obtained of the B , G , and Y for DC-HgGa₂Se₄ at zero pressure in the three approximations. The bulk modulus $B_H = 37.4$ GPa is in very good agreement with the value of $B_0 = 36.0$ GPa obtained from a third order Birch-Murnaghan EOS [53].

Table 7.3 includes the values of the ratio between the bulk and shear modulus, B/G , and the shear anisotropy factor A . According to the Pugh criterion [54], a B/G value above 1.75 indicates a tendency for ductility; otherwise, the material behaves in a brittle manner. The value of $B/G = 1.81$ indicates that the material should behave in a ductile manner. The shear anisotropy factor A for the tetragonal cell is defined as $A = 2C_{66} / (C_{11} - C_{12})$. If A is equal to one, no anisotropy exists. On the other hand, the more this parameter differs from one, the more elastically anisotropic is the crystalline structure. In this case the material shows an anisotropic behavior.

As mentioned previously, the elastic constants allow the study of the mechanical stability of the system. A lattice is mechanically stable only if the elastic energy change associated with an arbitrary deformation given by small strains is positive for any small deformation [55]. It means that the principal minors of the determinant with elements C_{ij} are all positive [56]. This is known as the Born stability criteria. For the case of a tetragonal crystal with six C_{ij} elastic constants, the mechanical stability at zero pressure requires that:

$$C_{11} > 0, \quad C_{44} > 0, \quad C_{66} > 0, \quad C_{11} - C_{12} > 0 \quad (7.9)$$

and

$$C_{11}C_{33} + C_{12}C_{33} - 2C_{13}^2 > 0 \quad (7.10)$$

DC-HgGa₂Se₄ at zero pressure satisfies the Born stability criteria and the crystal is mechanically stable at zero pressure [47]. Similarly, Ma et al. obtained the seven theoretical elastic constants at equilibrium pressure of DC-CdGa₂S₄ and DC-CdGa₂Se₄ using the pseudopotential plane wave method and the GGA approximation to describe the exchange correlation potential [49]. They concluded that also both compounds are mechanically stable at zero pressure.

To analyze the mechanical stability of a structure at high pressure it is necessary to study the evolution of the elastic constants as pressure increases and modify the Born stability criteria. The generalized Born stability criteria valid for the tetragonal crystal under an external hydrostatic pressure P take the form [56]:

$$C_{11} - P > 0, \quad C_{44} - P > 0, \quad C_{66} - P > 0, \quad (7.11)$$

$$C_{11} - C_{12} - 2P > 0 \quad (7.12)$$

$$(C_{33} - P)(C_{11} + C_{12}) - 2(C_{13} + P)^2 > 0 \quad (7.13)$$

The study of the mechanical stability of DC-HgGa₂Se₄ under pressure by Gomis et al. [47] concluded that the tetragonal phase becomes mechanically unstable beyond

Table 7.4 Theoretical and experimental cell parameters and Wyckoff positions of PC-CdIn₂Se₄ at zero pressure

	Theory			Experiment [58]		
a (Å)	5.7763			5.8151		
c (Å)	5.9042			5.80		
Wyckoff positions	x	y	z	X	y	z
Cd (<i>1a</i>)	0	0	0	0	0	0
In (<i>2f</i>)	0.5	0	0.5	0.5	0	0.5
Se (<i>4n</i>)	0.2776	0.2776	0.2281	0.2707	0.2707	0.230

13.3 GPa. Experimentally, this pressure is consistent with the pressure at which dark linear effects appear in optical absorption experiments.

7.7 Theoretical Study of CdIn₂Se₄ in the Pseudo-Cubic Phase

In order to illustrate how ab initio methods allow the study of OVCs in a predictive way, we present a theoretical study of PC-CdIn₂Se₄ under pressure [57]. This material has not been studied experimentally under pressure. Structural studies on polytypes of CdIn₂Se₄ have been reported by Ivaschchenko et al. [58], that include the tetragonal PC phase at zero pressure.

In the tetragonal PC structure, the primitive unit cell contains one formula unit; i.e., 7 atoms. Cd atoms are located at *2a* Wyckoff positions, In atoms at *2f* positions, and Se atoms at *4n* positions (*x*, *y*, *z*) with *x* = *y*. Therefore, in this structure there are two free lattice parameters (*a* = *b*, *c*) and two internal atomic positions of Se atoms (see Table 7.4). Alternatively, the PC phase is characterized by one external parameter *c/a*, and two internal parameters, *x* and *z*.

Total-energy ab initio simulations have been performed within DFT framework as implemented in the Vienna ab initio simulation package (VASP) [59, 60] (and references therein). The program performs ab initio structural calculations with the plane-wave pseudo-potential method. The set of plane waves employed extended up to a kinetic energy cutoff of 370 eV in order to achieve highly converged results within the projector-augmented-wave (PAW) scheme [60, 61]. The PAW method takes into account the full nodal character of the all-electron charge density distribution in the core region. The exchange-correlation energy was treated with the GGA-PBESol functional [48]. It is well known that the GGA approach typically underestimates the cohesion energy [5] (in turn producing an overestimation of the equilibrium volume). We used dense special point grids appropriate to the structure considered to sample the Brillouin zone (BZ), thus ensuring a high convergence of 1–2 meV per formula unit in the total energy of each structure as well as an accurate calculation of the forces on the atoms. At each selected volume, the structures were fully relaxed through the calculation of the forces on atoms and the stress tensor [5]. It means that

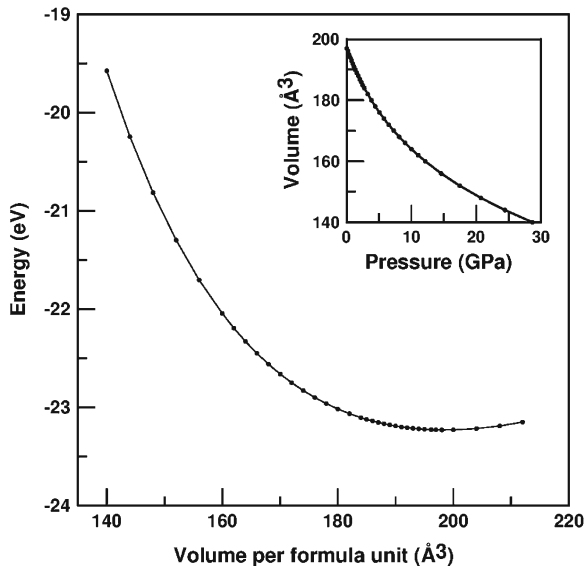


Fig. 7.3 Theoretical $E(V)$ and $V(P)$ data for PC- CdIn_2Se_4

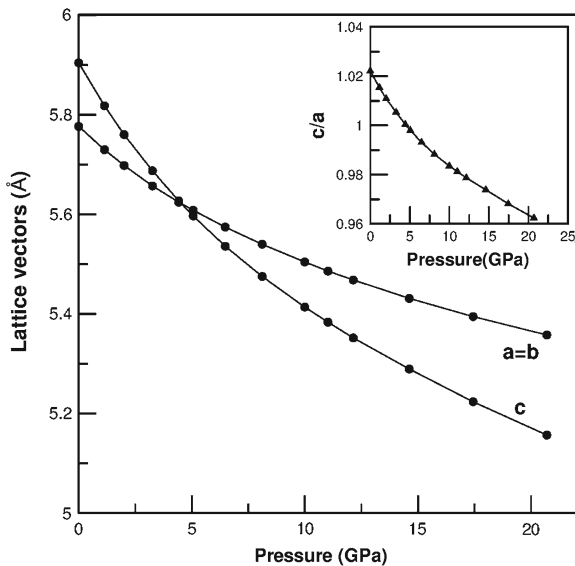
for a select volume, V , we obtain the theoretical $E(V)$ and $P(V)$ at the same time but independently. The equilibrium volume, V_0 , corresponds to the relaxed theoretical equilibrium (the V with lower E and $P = 0$) configuration. The forces were smaller than $0.006 \text{ eV}/\text{\AA}$, and the deviation of the stress tensor, from a diagonal hydrostatic form was less than 0.1 GPa in all the relaxed volumes.

Table 7.4 reports the calculated structural parameters at equilibrium, except for the typical overestimation of the GGA approach the theoretical results compare quite well with the available experimental parameters. Figure 7.3 shows the calculated energy versus volume data, the inset also shows the calculated evolution of volume with increasing pressure. These data are fitted with a Birch–Murnaghan 4th order EOS [53]. Values of bulk modulus and pressure derivatives are $B_0 = 33.2 \text{ GPa}$, $B'_0 = 4.7$ and $B''_0 = 0.4 \times 10^{-3}$. Figure 7.4 shows the pressure evolution of the calculated lattice parameters and c/a ratio. The axial compressibility for a and c axes at zero pressure are calculated as $\kappa_x = \frac{-1}{x} \frac{\partial x}{\partial p}$. We obtain $\kappa_a = 5.7 \times 10^{-3} \text{ GPa}^{-1}$, and $\kappa_c = 9.9 \times 10^{-3} \text{ GPa}^{-1}$, these values show an anisotropic compressibility, being c the most compressible axis according to our calculations.

Lattice-dynamics calculations of phonon modes were performed at the zone center (Γ point) of the BZ with the direct force-constant approach without the inclusion of electric field effects [10]. These calculations provide information about the symmetry of the modes and their polarization vectors, and allow us to identify the irreducible representations and the character of the phonon modes at the Γ point.

According to group theory, the PC structure of CdIn_2Se_4 has 21 phonon modes at Γ with the mechanical representation [41]:

Fig. 7.4 Pressure dependence of the theoretical lattice parameters a , c and c/a of PC-CdIn₂Se₄



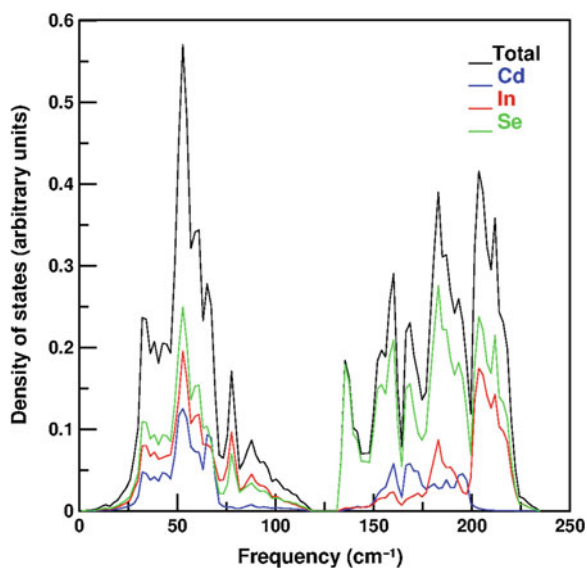
$$\Gamma = 2A_1(\text{R}) \oplus 2A_2 \oplus B_1(\text{R}) \oplus 4B_2(\text{R, IR}) \oplus 6E(\text{R, IR})$$

where A_1 and B_1 are non-polar modes, A_2 are silent modes, and B_2 and E are polar modes, being E modes doubly degenerated. This results in a total of 16 Raman-active modes ($2A_1 \oplus B_1 \oplus 3B_2 \oplus 5E$) and 13 IR-active modes ($3B_2 \oplus 5E$) since one B_2 and one E are acoustic modes. Table 7.5 summarizes the symmetries of the phonons along with their frequencies and pressure derivatives. The results were subsequently fitted to the polynomial $\omega(P) = \omega_0 + a \cdot P + b \cdot P^2$, where P is the pressure, ω_0 is the zero pressure frequency, and a and b are the first-order and second-order pressure coefficients. Figure 7.5 shows the total Phonon density of states (DOS) and the projected phonon density of states (PDOS) for each atom. The modes are located in two frequency regions, one from 0–120 cm^{-1} , and the other from 130–230 cm^{-1} , clearly separated by a phonon-gap. The main contribution to vibrations above 130 cm^{-1} comes from the Se atom, due to the lower mass of this atom. Figure 7.6 shows the pressure evolution of the calculated phonon modes. A dynamical instability appears around 18 GPa because both the silent A_2 mode and the E mode with lowest frequency become negative. The softening of these modes could be the fingerprint of a phase transition around that pressure which is similar to the phase transition pressures found in other OVCs of the AB_2X_4 family (see Chaps. 5 and 6 of this book).

We include the effect of the electric field in our calculations by means of the Born-effective charge tensor, and the dielectric constant calculated from ab initio. As already commented, this procedure allows us to include the non-analytical term at the Γ point and to calculate the LO–TO splitting of the polar modes B_2 and E .

Table 7.5 Theoretical frequencies of Raman, Infrared and silent modes and pressure coefficients of PC-CdIn₂Se₄ as obtained from fits to the data using $\omega = \omega_0 + aP + bP^2$ equation

Mode symmetry	ω_0 (cm ⁻¹)	a (cm ⁻¹ GPa ⁻¹)	b (cm ⁻¹ GPa ⁻²)
E(RI)	49.50	-0.77 ^a	-0.051 ^a
A ₂	52.10	-1.24 ^b	-0.043 ^b
B ₂ (RI)	65.75	-0.26	-0.017
E (RI)	77.92	-0.41	0.005
A ₁ (R)	138.50	4.78	-0.044
B ₂ (RI)	160.05	3.86	-0.058
E (RI)	175.80	3.20	-0.024
E (RI)	179.17	4.53	-0.066
A ₁ (R)	183.33	3.58	-0.053
B ₁ (R)	183.33	3.32	-0.033
E (RI)	206.05	4.39	-0.058
A ₂	206.22	4.15	-0.052
B ₂ (RI)	210.89	2.89	-0.029

^a Fit up to 18 GPa^b Fit up to 14 GPa**Fig. 7.5** Calculated phonon total density of states (DOS) and atom projected DOS of PC-CdIn₂Se₄

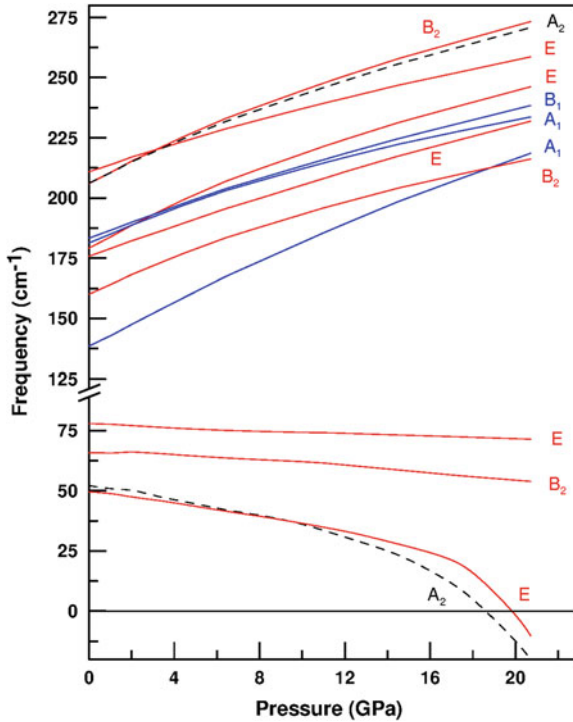


Fig. 7.6 Pressure dependence of the theoretical Raman, IR and silent modes of PC-CdIn₂Se₄

Figure 7.7 displays the phonon dispersion at zero pressure of PC-CdIn₂Se₄, showing the LO–TO splitting of the different modes at the Γ point.

Finally, we have studied the elastic properties of PC-CdIn₂Se₄. As already commented, the PC structure has six independent second-order elastic constants which are: C_{11} , C_{12} , C_{13} , C_{33} , C_{44} , and C_{66} . Table 7.6 reports the calculated values of the C_{ij} elastic constants as well as the shear modulus, G , the Young modulus, Y , the Poisson's ratio (ν), and other calculated elastic parameters (see (7.1–7.8)). We obtain a bulk modulus of 34.5 GPa, a shear modulus G_v of 18.76 GPa and a Young modulus Y_v of 47.7 GPa. Note that the reported B_v bulk modulus obtained from the elastic constants 34.8 GPa, agrees with the B obtained from the Birch–Murnaghan 4th EOS fit [53], this gives confidence to our elastic constants calculation. The ratio between bulk modulus and shear modulus ($B/G = 1.86$) indicates that the compound is ductile according to the Pugh criteria. The shear anisotropy factor ($A = 3.6$) is clearly different of one, thus indicating a clear anisotropy of this compound.

At zero pressure the Born stability criteria are fulfilled for PC-CdIn₂Se₄ and the crystal is mechanically stable. Figure 7.8 shows the pressure evolution of the C_{ij} elastic constants. C_{11} , C_{12} , C_{33} , and C_{13} increase monotonically as pressure increase, whereas C_{44} and C_{66} increase with pressure up to 10 and 5 GPa, respectively, and then

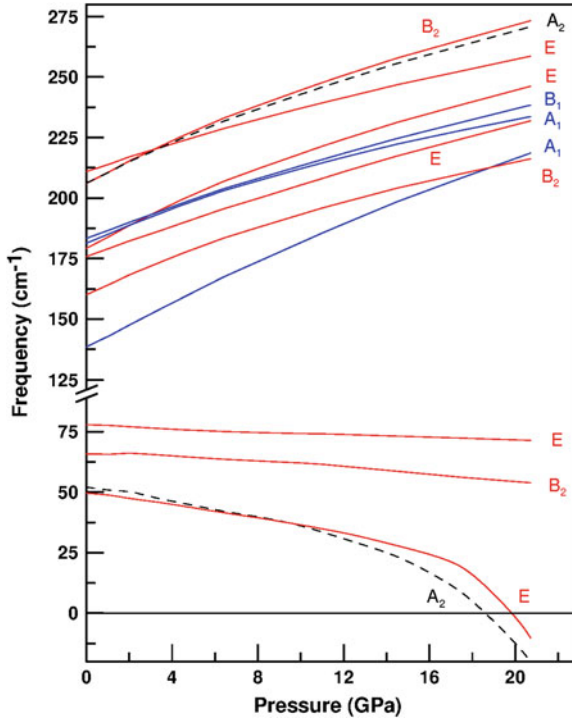


Fig. 7.7 Theoretical phonon dispersion at zero pressure for PC-CdIn₂Se₄ (LO-TO splitting at Γ point is included)

decrease as pressure increase. These results allow us to study the mechanical stability under pressure. The generalized Born criteria of this compound under pressure are represented in Fig. 7.9. It is clear that above 11 GPa two of the generalized Born criteria, defined by (7.12) and (7.13), are violated; therefore, the system becomes mechanically unstable above this pressure. This pressure is similar to the pressure for which the calculated elastic constant C_{44} begins to decrease, but lower than the pressure at which the dynamic instability appears. It remains to be checked experimentally if the different pressures for mechanic and dynamic instability of PC-CdIn₂Se₄ could be related to the occurrence of phase transitions and to the appearance of dark linear defects which are precursors of the phase transition to an opaque metallic phase as the DR phase observed in several OVCs.

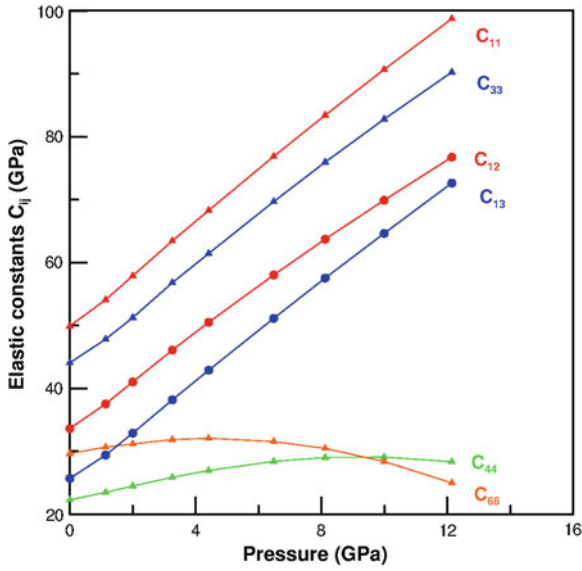


Fig. 7.8 Calculated pressure evolution of the C_{ij} elastic constants of PC-CdIn₂Se₄

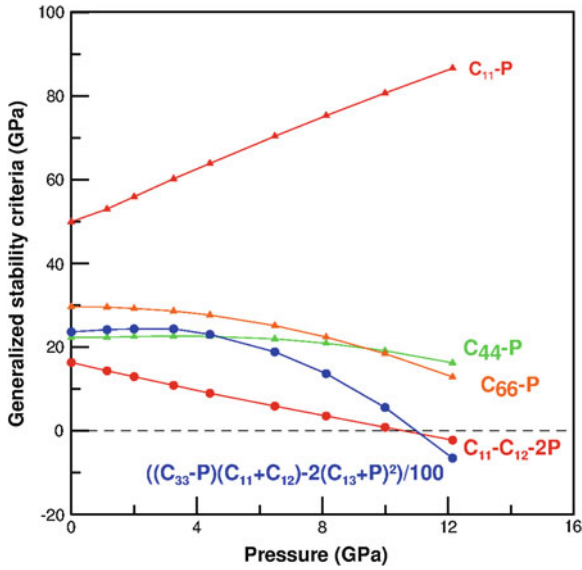


Fig. 7.9 Generalized Born stability criteria as function of pressure for PC-CdIn₂Se₄

Table 7.6 Elastic constants C_{ij} (in GPa) for PC-CdIn₂Se₄. Bulk (B_v), shear (G_v), and Young (Y_v) moduli (in GPa), Poisson's ratio (ν_v), B_v/G_v ratio, and shear anisotropy factor (A_v) are also given in the Voigt approximation

C_{11}	C_{33}	C_{44}	C_{66}	C_{12}	C_{13}	B_v	G_v	E_v	ν_v	B_v/G_v	A_v
49.9	44.1	22.3	29.6	33.6	25.7	34.5	18.8	47.7	0.27	1.86	3.64

7.8 Conclusions

In this chapter we have made an overview of the electronic, elastic, and vibrational properties of the OVCs of the AB₂X₄ (X = S, Se) family under pressure from a theoretical point of view. *First principles* (also known as ab initio) calculations are a powerful complement to experimental results. These studies can predict many properties of the materials under extreme conditions that sometimes are not available from experiments. Although theoretical studies are scarce, e.g. there is no work published on OVCs with X = Te, they may help to elucidate some controversy on the structural, electronic, elastic, and vibrational properties under pressure. We also presented a theoretical study of the pseudo-cubic CdIn₂Se₄ under pressure, where no experimental data under pressure are available. We hope this overview will encourage further studies that cover the lack of data on OVCs under pressure.

References

1. Hohenberg P, Kohn W (1964) Inhomogenous electron gas. *Phys Rev* 136:B864–B871
2. Kohn W, Sham LJ (1965) Self-consistent equations including exchange and correlation effects. *Phys Rev* 140:A1133–A1138
3. Payne MC, Teter MP, Allan DC, Arias TA, Joannopoulos JD (1992) Iterative minimization techniques for ab initio total-energy calculations: molecular dynamics and conjugate gradients. *Rev Mod Phys* 64:1045–1097
4. Martin RM (2004) *Electronic structure: basic theory and practical methods*. Cambridge University Press, New York
5. Mujica A, Rubio A, Muñoz A, Needs RJ (2003) High pressure phase of group-IV, III-V, and II-VI compounds. *Rev Mod Phys* 75:863–912
6. Nielsen OH, Martin RM (1983) First-principles calculations of stress. *Phys Rev Lett* 50:697–700
7. Pickard CJ, Needs RJ (2011) Ab initio random structure searching. *J Phys:Condens Matter* 23:053201(23)
8. Oganov A, Ma YM, Lyakhov AO, Valle M, Gatti C (2010) Evolutionary crystal structure prediction as a method for the discovery of minerals and materials, in theoretical and computational methods in mineral physics: geophysical applications. In: Wentzcovitch R, Stixrude L (eds) *Reviews in mineralogy & geochemistry*, vol 71. New York, McGraw-Hill, pp 271–298
9. Baroni S, de Gironcoli S, Dal Corso A, Gianozzi P (2001) Phonons and related crystal properties from density-functional perturbation theory. *Rev Mod Phys* 73:515(48)
10. Parlinski K (1999) Calculation of phonon dispersion curves by the direct method. In: Johnson MR, Kearley GJ, Buttner HG (eds) *Neutrons and numerical methods-n(2)m*. AIP conference proceedings, vol 479. New Yorks, AIP, pp 121–126

11. Alfe D (2009) PHON: a program to calculate phonons using the small displacement method. *Comp Phys Commun* 180:2622–2633
12. Bhosale J, Ramdas AK, Burger A, Muñoz A, Romero AH, Cardona M, Lauck R, Kremer RK (2012) Temperature dependence of band gaps in semiconductors: electron–phonon interaction. *Phys Rev B* 86:195208(10)
13. Georgobiani AN, Radaustan SI, Tiginyanu IM (1985) Wide-gap A(II)B(III)₂C(VI)₄ semiconductors—optical and photoelectric properties, and potential applications (review). *Sov Phys Sem (USSR)* 19:121–132
14. Bernard JE, Zunger A (1988) Ordered-vacancy-compound semiconductors:pseudocubic CdIn₂Se₄. *Phys Rev B* 37:6835–6856
15. Fahy S, Chang KJ, Louie SG, Cohen ML (1987) Pressure coefficients of band-gaps of diamond. *Phys Rev B* 35:5856–5859
16. Baldereschi A, Meloni F, Aymerich F, Mula G (1977) Electronic properties of defect-Zincblende semiconductor CdIn₂Se₄. *Solid State Commun* 21:113–116
17. Marinelli M, Depascale T, Meloni F, Mula G, Serra M, Baroni S (1989) Theoretical-study of cubic versus tetragonal structures of defect Zincblende semiconductors—CdIn₂Se₄. *Phys Rev B* 40:1725–1731
18. Jiang XS, Lambrecht WRL (2004) Electronic band structure of ordered vacancy defect chalcopyrite compounds with formula II-III₂-VI₄. *Phys Rev B* 69:035201(8)
19. Mishra S, Ganguli B (2011) Electronic and structural properties of a Al₂Se₄ (A=Ag, Cu, Cd, Zn) chalcopyrite semiconductors. *J Solid State Chem* 184:1614–1621
20. Fuentes-Cabrera M, Sankey OF (2001) Theoretical study of the ordered-vacancy semiconducting compound CdAl₂Se₄. *J Phys: Condens Matter* 13:1669–1684
21. Perdew JP, Zunger A (1981) Self-interaction correction to density-functional approximations for many-electron systems. *Phys Rev B* 23:5048–5079
22. Perdew JP (1991) Generalized gradient approximations for exchange and correlation—a look backward and forward. *Physica B* 172:1–6
23. Fritsche L, Gu YM (1993) Band gaps in a generalized density-functional theory. *Phys Rev B* 48:4250–4258
24. Ouahrani T, Reshak AH, Khenata R, Amrani B, Mebrouki M, Otero-de-la-Roza A, Luana V (2010) Ab-initio study of the structural, linear and nonlinear optical properties of CdAl₂Se₄ defect-chalcopyrite. *J Solid State Chem* 183:46–51
25. Engel E, Vosko SH (1993) Exact exchange-only potentials and the virial relation as microscopic criteria for generalized gradient approximations. *Phys Rev B* 47:13164–13174
26. Verma UP, Singh P, Jensen P (2012) Pressure and temperature induced structural, electronic and thermal properties of CdAl₂Se₄. *Solid State Commun* 152:624–629
27. Perdew JP, Burke K, Ernzerhof M (1996) Generalized gradient approximation made simple. *Phys Rev Lett* 77:3865–3868
28. Verma UP, Singh P, Jensen P (2011) A study of the electronic, optical and thermal properties for ZnAl₂Se₄ using the FP-LAPW method. *Phys Stat Solidi B* 248:1682–1689
29. Jiang X-S, Yan Y-C, Yuan S-M, Mi S, Niu Z-G, Lian J-Q (2010) Trends in the band-gap pressure coefficients and bulk moduli in different structures of ZnGa₂S₄, ZnGa₂Se₄, and ZnGa₂Te₄. *Chin Phys B* 19:107104(7)
30. Ouahrani T, Khenata R, Lasri B, Reshak AH, Bouhemadou A, Bin-Omran S (2012) First and second harmonic generation of the XAl₂Se₄ (X = Zn, Cd, Hg) defect chalcopyrite compounds. *Physica B* 407:3760–3766
31. Singh P, Verma UP, Jensen P (2011) Electronic and optical properties of defect chalcopyrite HgAl₂Se₄. *J Phys Chem Solids* 72:1414–1418
32. Reshak AH, Khenata R, Kityk IV, Plucinski KJ, Auluck S (2009) X-ray photoelectron spectrum and electronic properties of a noncentrosymmetric chalcopyrite compound HgGa₂S₄: LDA, GGA, and EV-GGA. *J Phys Chem B* 113:5803–5808
33. Lavrentyev AA, Gabrelian BV, Dubeiko VA, Nikiforov IY, Rehr JJ (2002) Experimental and theoretical X-ray K spectra of sulfur of zincblende-based compounds AgGaS₂ – CdGa₂S₄ – InPS₄. *J Phys Chem Solids* 63:227–231

34. Lavrentyev AA, Gabrelian BV, Nikiforov IY, Rehr JJ, Ankudinov AL (2003) Ab initio calculations of the electron structure of the compounds AgGaS_2 , CdGa_2S_4 , InPS_4 . *J Phys Chem Solids* 64:1251–1255
35. Lavrentyev AA, Gabrelian BV, Nikiforov IY, Parasyuk OV, Khyzhun OY (2009) Electronic structure of cadmium selenogallate CdGa_2Se_4 as studied using ab initio calculations and X-ray photoelectron spectroscopy. *J Alloys Comp* 481:28–34
36. Fuentes-Cabrera M (2001) Ab initio study of the vibrational and electronic properties of CdGa_2S_4 and CdGa_2Se_4 under pressure. *J Phys: Condens Matter* 13:10117–10124
37. Manjón FJ, Gomis O, Rodríguez-Hernández P, Pérez-González E, Muñoz A, Errandonea D, Ruiz-Fuertes J, Segura A, Fuentes-Cabrera M, Tiginyanu IM, and Ursaki VV (2010) Nonlinear pressure dependence of the direct band gap in adamantine ordered-vacancy compounds. *Phys Rev B* 81:195201(7)
38. Gomis O, Vilaplana R, Manjón FJ, Pérez-González E, López-Solano J, Rodríguez-Hernández P, Muñoz A, Errandonea D, Ruiz-Fuertes J, Segura A, Santamaría-Pérez D, Tiginyanu IM, Ursaki VV (2012) High-pressure optical and vibrational properties of CdGa_2Se_4 : order–disorder processes in adamantine compounds. *J Appl Phys* 111:013518(15)
39. Ohrendorf FW, Haeuseler H (1995) Lattice dynamical calculations on compounds crystallizing in a Thiogallate-type structure. *J Solid State Chem* 114:442–450
40. Ursaki VV, Burlakov II, Tiginyanu IM, Raptis YS, Anastassakis E, Anedda A (1999) Phase transitions in defect chalcopyrite compounds under hydrostatic pressure. *Phys Rev B* 59:257–268
41. Manjón FJ, Gomis O, Vilaplana R, Sans JA, Ortiz HM (2013) Order–disorder processes in adamantine ternary ordered-vacancy compounds. *Phys Stat Sol B* (in press). doi:[10.1002/pssb.201248596](https://doi.org/10.1002/pssb.201248596)
42. Vilaplana R, Robledillo M, Gomis O, Sans JA, Manjón FJ, Pérez-González E, Rodríguez-Hernández E, Muñoz A, Tiginyanu IM, Ursaki VV (2013) Vibrational study of HgGa_2S_4 under high pressure. *J Appl Phys* 113:093512(10)
43. Vilaplana R, Gomis O, Manjón FJ, Ortiz H, Pérez-González E, Ortiz HM, Rodríguez-Hernández P, Muñoz A, Errandonea D, Ursaki VV, Tiginyanu IM (2013) Lattice dynamics study of HgGa_2Se_4 at high pressures (to be published)
44. Vilaplana R, Gomis O, Pérez-González E, Ortiz HM, Manjón FJ, Rodríguez-Hernández P, Muñoz A, Alonso-Gutiérrez P, Sanjuán ML, Ursaki VV, Tiginyanu IM (2013) Thermally activated cation ordering in ZnGa_2Se_4 single crystals studied by Raman scattering, optical absorption, and ab initio calculations. *J Phys: Condens Matt* 25:165802(11)
45. Nye JF (1957) *Physical properties of crystals: their representation by tensors and matrices*. Oxford University Press, Oxford
46. Farley JM, Saunders GA, Chung DY (1973) Elastic-constants of strontium molybdate. *J Phys C: Solid State Phys* 6:2010–2019
47. Gomis O, Vilaplana R, Manjón FJ, Santamaría-Pérez D, Errandonea D, Pérez-González E, López-Solano J, Rodríguez-Hernández P, Muñoz A, Tiginyanu IM, Ursaki VV (2013) High-pressure study of the structural and elastic properties of defect-chalcopyrite HgGa_2Se_4 . *J Appl Phys* 113:073510(10)
48. Perdew JP, Ruzsinszky A, Csonka GI, Vydrov OA, Scuseria GE, Constantin LA, Zhou X, Burke K (2008) Restoring the density-gradient expansion for exchange in solids and surfaces. *Phys Rev Lett* 100:136406(4)
49. Ma S-H, Jiao Z-Y, Zhang X-Z (2012) Structural, elastic, electronic, and optical properties of defect-chalcopyrite structure CdGa_2X_4 ($\text{X} = \text{S}, \text{Se}$) compounds. *J Matt Sci* 47:3849–3854
50. Voigt W (1928) *Lehrbuch der Kristallphysics*. Teubner, Leipzig
51. Reuss A, Anew Z (1929) Account of the liquid limit of mixed crystals on the basis of the plasticity condition for single crystal. *Angew Math Mech* 9:49–58
52. Hill R (1952) The elastic behavior of a crystalline aggregate. *Proc Phys Soc London, Sect A* 65:349–355
53. Birch F (1947) Finite elastic strain of cubic crystals. *Phys Rev* 71:809–824

54. Pugh SF (1954) Relations between the elastic moduli and the plastic properties of polycrystalline pure metals. *Philos Mag* 45:823–843
55. Born M, K'un H (1954) *Dynamical theory of crystal lattices*. Oxford University Press, Oxford
56. Wallace DC (1972) *Thermodynamics of crystals*. Wiley, New York
57. Muñoz A, Rodríguez-Hernández P (2013) Theoretical Ab Initio Calculations in Ordered Vacancy Compounds at High Pressures. In: Manjon FJ, Tiginyanu IM, Ursaki VV (ed) *Pressure-Induced Phase Transitions in AB₂X₄ Chalcogenides Compounds*, Springer Series in Materials Science, Springer-Verlag Berlin Heidelberg
58. Ivaschchenko IA, Aksel'rud LG, Olekseyuk ID, Zmii OF (2004) *Ukrains'kii Khimicheskii Zhurnal (Russian Edition)* 70:67–71
59. Kresse G, Furthmüller J (1996) Efficient iterative schemes for ab initio total-energy calculations using a plane-wave basis set. *Phys Rev B* 54:11169–11186
60. Kresse G, Joubert D (1999) From ultrasoft pseudopotentials to the projector augmented-wave method. *Phys Rev B* 59:1758–1775
61. Blochl PE (1994) Projector augmented-wave method. *Phys Rev B* 50:17953–17979